Radical Enhanced Charge Transport in Single-Molecule Phenothiazine Electrical Junctions

Junyang Liu[#], Xiaotao Zhao[#], Qusiy Al-Galiby[#], Xiaoyan Huang, Jueting Zheng, Ruihao Li, Cancan Huang, Yang Yang, Jia Shi, David Zsolt Manrique, Colin Lambert*, Martin R. Bryce*, Wenjing Hong*

This manuscript is dedicated to the memory of Professor Thomas Wandlowski.

Abstract: We studied the single-molecule conductance through an acid oxidant triggered phenothiazine (PTZ) based radical junction using the Mechanically Controllable Break Junction technique. The electrical conductance of the radical state was enhanced by up to 200 times compared to the neutral state, with high stability lasting for at least two months and high junction formation probability at room-temperature. Theoretical studies revealed that the conductance increase is due to a significant decrease of the HOMO-LUMO gap and also the enhanced transmission close to the HOMO orbital when the radical forms. The large conductance enhancement induced by the formation of the stable PTZ radical molecule will lead to promising applications in single-molecule electronics and spintronics.

Investigations of charge transport through single molecules provide vital information for the design of materials for next-generation electronic devices.[1] Recently, all-organic radical

[*]　Dr. Junyang Liu[#], Xiaoyan Huang, Jueting Zheng, Ruihao Li, Dr. Yang Yang, Dr. Jia Shi, Prof. Dr. Wenjing Hong
State Key Laboratory of Physical Chemistry of Solid Surfaces, Department of Chemical and Biochemical Engineering, College of Chemistry and Chemical Engineering, Graphene Industry and Engineering Research Institute, iChEM, Xiamen University
Xiamen 361005, China
E-mail: whong@xmu.edu.cn
Dr. Xiaotao Zhao[#], Prof. Martin R. Bryce
Department of Chemistry, Durham University
Durham DH1 3LE, United Kingdom
E-mail: m.r.bryce@durham.ac.uk
Qusiy Al-Galiby[#], David Zsolt Manrique, Prof. Colin Lambert
Department of Physics, Lancaster University
Lancaster LA1 4YB, United Kingdom
E-mail: c.lambert@lancaster.ac.uk
Dr. Junyang Liu, Dr. Cancan Huang, Dr. Wenjing Hong
Department of Chemistry and Biochemistry, University of Bern
Freiestrasse 3, CH-3012 Bern, Switzerland
Qusiy Al-Galiby
Department of Physics, College of Education, University of Al-Qadisiyah, Iraq
Al-Qadisiyah, Diwaniya city, 58002, Iraq
Dr. David Manrique
Department of Electronic & Electrical Engineering, University College London
Torrington Place, London WC1E 7JE, United Kingdom

[#]　These authors contributed equally to this work

Supporting information for this article is given via a link at the end of the document.

species have raised broad interest as the unpaired electron can lead to novel quantum phenomena for the electronics properties tuning,[2] such as Kondo effects,[3] quantum interference[4] and magnetoresistive effects.[5] However, although some pioneering studies investigated the charge transport through radicals using molecular assemblies[5a, 6] or under ultra-high vacuum and cryogenic environment,[3b, 5b] the seeking of appropriate molecular radicals for the fabrication of stable and highly conductive single-molecule devices remained as a major challenge for applying molecular radicals for future electronics devices.

The phenothiazine (PTZ) system can undergo one-electron oxidation on the nitrogen atom to form a radical cation (PTZ[+•])[7] with accompanying significant color change in solution via adding acid oxidant such as trifluoroacetic acid (TFA) under ambient conditions. More interestingly, the butterfly structure of the PTZ became more planar for the radical cation with electron density delocalized over the whole molecule including the central ring.[8] Such prominent changes in the electronic properties of the PTZ radicals have received increasing research interests in organic light-emitting diodes,[9] and also offer promising applications in the radical based molecular electronics devices.
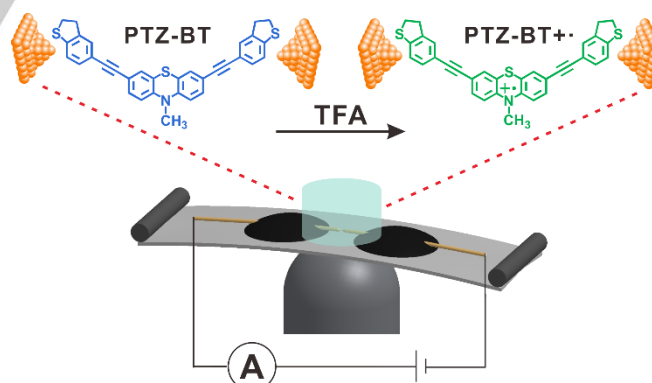
Scheme 1. Schematic of MCBJ setup and radical trigger reaction of PTZ derivative.

Herein, we study the single-molecule conductance of a PTZ derivative and its corresponding radical cation using the Mechanically Controllable Break Junction (MCBJ) technique[10] in a mixed tetrahydrofuran/1,3,5-trimethylbenzene (THF/TMB, 1:4 *v/v*) solution at room temperature, as shown in Scheme 1. Prominent conductance signals of both the PTZ derivative and

its corresponding radical cation are observed with a large conductance enhancement of up to 200 times for the radical state. Theoretical studies also reproduced the results that the radical state possesses a significantly higher electrical conductance compared with the neutral state because of significant electronic structural changes.

The PTZ derivative (10-Methyl-PTZ) named as **PTZ-BT** was designed and synthesized with dihydrobenzo[*b*]thiophene (BT) as the anchoring groups (See Supporting Information (SI) section 1 for synthetic details).[11] The radical cation 10-Methyl-PTZ$^{+\bullet}$ named as **PTZ-BT+•** was triggered upon adding 20% volume TFA into a THF/TMB solution of the neutral **PTZ-BT**.[12] To confirm the existence of the radical cation, UV-Vis absorption and Electron Spin Resonance (ESR) spectra were used to monitor the changes after TFA addition. The light-green solution of **PTZ-BT** turned pink immediately after the addition, and an absorption band around 518 nm emerged, as shown in Figure 1a. This absorption band suggested a $\pi \rightarrow \pi^*$ transition, which has been shown previously to be a signature of the phenothiazine radical cation.[12d, 13] Furthermore, Figure 1b shows the ESR spectra of the solution of **PTZ-BT** before and after adding TFA: a distinct radical signal with 6 hyperfine splitting lines is observed after the addition. This splitting pattern, with g values close to 2.0051, is consistent with the literature data for a single unpaired electron on the nitrogen atom of the PTZ ring, suggested the generation of **PTZ-BT+•**.[12a, 14]
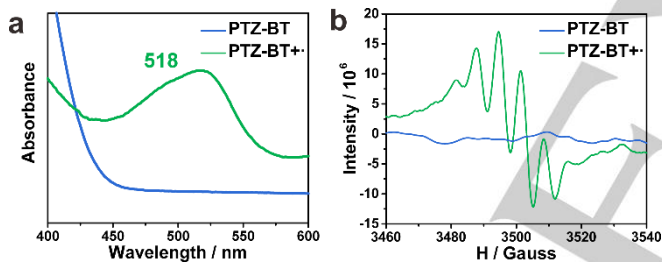

Figure 1. The (a) UV-Vis absorption spectra and (b) ESR spectra of PTZ species in THF/TMB mixed solution, before (blue) and after (green) the addition of TFA.

Single-molecule conductance data were measured using the MCBJ technique in the mixed THF/TMB solution as mentioned above with a 0.1 mM concentration of the phenothiazine derivatives, and 100 mV bias voltage was applied between the two electrodes (See SI section 2 for more details of conductance measurements).[10a, 10b, 15] Figure 2a shows the typical conductance traces of **PTZ-BT** and **PTZ-BT+•**. Both of the states exhibited clear molecular plateaus after discrete G_0 steps (where G_0 is the conductance quantum which equals $2e^2/h$), which suggests a gold atomic chain is pulled out then a molecular junction is formed.[1c] Although the curves of **PTZ-BT+•** showed higher tunneling background due to the higher ion concentration from the acid, conspicuous and stable conductance plateaus can be observed. Figure 2b shows the conductance histograms of both the neutral **PTZ-BT** and its corresponding radical cation states **PTZ-BT+•**; each was constructed from two thousand individual conductance traces from Figure 2a. Statistical results exhibited the conductance increases from the neutral state of

PTZ-BT as $10^{-5.1}$ G_0 (7.94×10^{-6} G_0) to the radical state of **PTZ-BT+•** as $10^{-2.8}$ G_0 (1.58×10^{-3} G_0), which suggest a remarkable conductance enhancement of up to 200 times. Control experiments of measuring merely TFA, and the tolane with BT anchors (OPE2-BT) mixed with TFA suggested that the conductance changes are neither from the TFA itself nor from the solvent tuning effect (See Figures S3 and S4 of SI for more details).[16]

The high enhancement ratio (200 times) of PTZ radical conductance even exceeded the highest enhancement ratio of the radical junction of the polychlorotriphenylmethyl radical SAM monolayer[6] recently reported by Yuan *et al.*, which shows an enhancement ratio up to 100 times for the radical molecule compared with the neutral one. More importantly, the enhanced conductance of the radical state of PTZ is even higher than that of the widely studied fully-conjugated oligophenyleneethynylene-3 (OPE3-SH, $10^{-3.7}$ G_0)[17] and even close to OPE2 (OPE2-SH, $10^{-2.8}$ G_0),[17a, 18] although **PTZ-BT+•** has a slightly longer molecular length than OPE3 (~2.0 nm), and is much longer than OPE2 (~1.3 nm).[17a] The comparison suggests that the PTZ core at the radical state is one of the most conductive molecular building blocks.
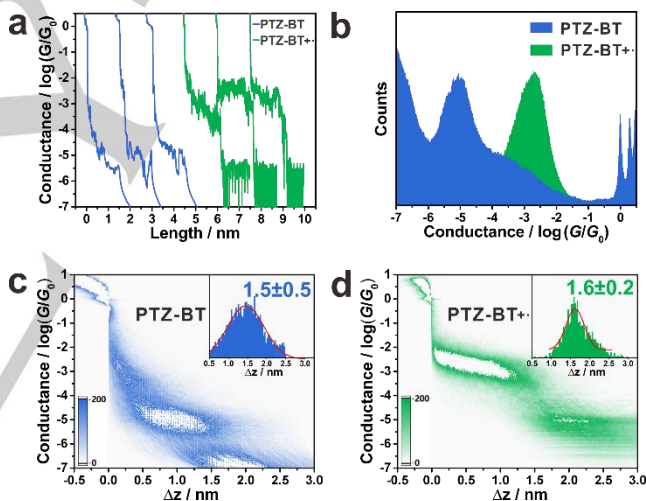

Figure 2. (a) Typical measured conductance distance traces of phenothiazine derivative **PTZ-BT** and its corresponding triggered radical cation **PTZ-BT+•**. (b) conductance histogram comparisons between both states before and after TFA addition. All-data-point 2D conductance versus relative distance (Δz) histogram and relative displacement distribution (inset) of (c) **PTZ-BT** and (d) **PTZ-BT+•**, the conductance ranges to determine the relative displacement distribution are from $10^{-0.3}$ to $10^{-6.0}$ G_0 for **PTZ-BT** and from $10^{-0.3}$ to $10^{-4.5}$ G_0 for **PTZ-BT+•**, respectively.

To further extract the effect of configuration changes on the charge transport through PTZ molecules, two-dimensional conductance-distance histograms[10a, 19] were constructed for each state without any data selection, as shown in Figures 2c and Figure 2d, with each of their relative displacement distributions shown as the upright insets. All the histograms showed unambiguous conductance clouds, indicating a high junction formation probability. It is found that the traces of **PTZ-BT** start with the direct tunnelling feature before the molecular plateau,[20] while the **PTZ-BT+•** conductance plateau appeared immediately after the rupture of the gold-gold contact. The

relative displacement distribution enlarged very slightly from the neutral state into the radical state (1.5 nm of **PTZ-BT** to 1.6 nm of **PTZ-BT+•**), for which the statistical range was from $10^{-0.3}$ to $10^{-6.0}$ G_0 for **PTZ-BT** and from $10^{-0.3}$ to $10^{-4.5}$ G_0 for **PTZ-BT+•**, respectively. When adding the 0.5 nm snap-back distance,[10a, 21] the length of the molecular junction is 2.0 and 2.1 nm for **PTZ-BT** and **PTZ-BT+•**, respectively, which are slightly less than the maximum possible values, based on the computed molecular lengths of 2.31 nm and 2.33 nm for **PTZ-BT** and **PTZ-BT+•** obtained from DFT simulations, respectively (See Figure S6-1 of SI for more details). These data suggest that these PTZ derivatives, especially the PTZ radical cation, possess relatively rigid structures to endure almost full stretching before junction breakage. The DFT simulations also suggest that the neutral and radical cation states have very similar molecular structures, with the dihedral angle of the PTZ core increased slightly from **PTZ-BT** to **PTZ-BT+•** (See Figure S6-2 of SI for more details). [8b, 22]
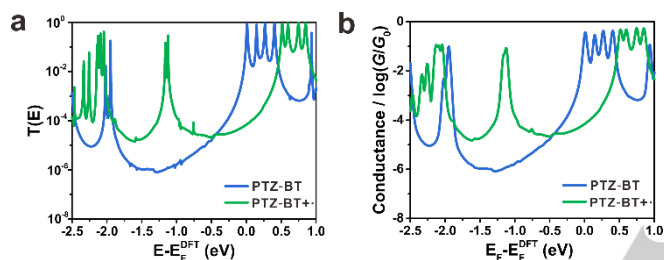

Figure 3. (a) Averaged spin-up and spin-down transmission coefficients of the two states, (b) room-temperature electrical conductance over a range of Fermi energies of two states. The blue lines refer to **PTZ-BT** and green to **PTZ-BT+•**, respectively.

Such a small conformational change cannot explain the large conductance enhancement. To understand the radical-enhanced charge transport phenomena, we used the density functional theory code SIESTA[23] to optimize the gold-molecule-gold junction geometry, and calculated the DFT mean-field Hamiltonian of the **PTZ-BT** molecules attached to two gold leads (with TFA placed close to **PTZ-BT** molecule for **PTZ-BT+•**). The GOLLUM quantum transport code,[24] was then used to obtain the electron transmission coefficient T(E) and room-temperature electrical conductance (See SI section 6-2 for more details). As shown in Figure 3, the HOMO-LUMO gap decreases from ~2 eV for **PTZ-BT** (blue curve) to ~1.6 eV for **PTZ-BT+•** (green curve), which is also confirmed by the red-shift of the UV-Vis spectra from Figure 1a.[25] The decrease of the HOMO-LUMO gap with approximately the same tunnelling distance (as shown in Figure 2c, 2d and Figure S6-1 in SI) leads to significant conductance enhancement due to the lower tunnelling barrier.[6] Moreover, it is also found that the transmission of **PTZ-BT+•** is significantly higher than that of **PTZ-BT** within a wide energy level range close to the HOMO of **PTZ-BT** (from -1.2 eV to -1.8 eV) and **PTZ-BT+•** (from -0.5 eV to -1.1 eV). Previous studies have shown that the charge transport through molecules with BT or thiol anchors is dominated by the HOMO, theoretically and experimentally.[11, 26] Although the exact alignment of the Fermi energy is still difficult to determine theoretically (See SI section

6-2 and 7 for more details and discussion),[16b, 21b, 27] the calculation still suggested that **PTZ-BT+•** exhibited higher conductance than **PTZ-BT** within the wide range of HOMO dominated energy levels. The agreement between the calculation and the single-molecule conductance measurements suggests that the conductance enhancement originates from the significant electronic structural changes of the PTZ core as the radical cation forms.

To further examine the long-term stability of the PTZ radical in solution, Figure 4 shows the conductance measurements of the **PTZ-BT+•** solution every 12 hours for two days, and the result from the measurement of the same solution after 2 months' storage (See Figure S5-1 of SI for more details). The conductance of **PTZ-BT+•** remained constant, which implies that the radical cation can exist at least for more than two months at room temperature in solution. The obtained UV-Vis spectra also revealed the presence of a radical species after long-period storage (See Figure S5-2 of SI for more details). Since organic radicals which consist of light elements such as H, C, N and S are promising materials due to the low spin-orbit coupling, they possess the potential to realize long spin relaxation times to enhance the stability of molecular devices.[2] Hence, due to the delocalization of the electron density through the phenothiazine radical core, the energy of the corresponding frontier molecular orbitals of the PTZ radical will be significantly lowered, therefore the stability of the radical system will be enhanced.[12a]
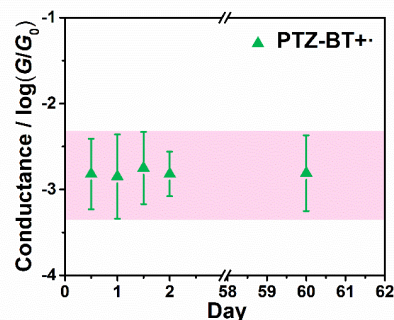

Figure 4. Measured conductance results of the radical cation **PTZ-BT+•** during two days and even two months after adding TFA. The light pink area suggests the long term stability of the single-molecule conductance of the PTZ radical.

In summary, we investigated the charge transport properties through a room temperature stable radical system with a phenothiazine core using single-molecule conductance measurements and density functional theory. Up to 200 times conductance enhancement has been observed for the radical state compared to the neutral state, with high stability and junction formation probability. DFT simulations show that the conductance increase is due to a significant decrease of the HOMO-LUMO gap and enhanced transmission close to the HOMO orbital when the radical forms. The significant conductance enhancement from the formation of the radical at room temperature leads to promising applications of PTZ molecules for single-molecule electronics, optoelectronics and spintronics studies.

Acknowledgements

[1] a)D. Xiang, X. Wang, C. Jia, T. Lee, X. Guo, *Chem. Rev.* **2016**, *116*, 4318-4440; b)N. J. Tao, *Nat. Nanotechnol.* **2006**, *1*, 173-181; c)C. Huang, A. V. Rudnev, W. Hong, T. Wandlowski, *Chem. Soc. Rev.* **2015**, *44*, 889-901; d)T. A. Su, M. Neupane, M. L. Steigerwald, L. Venkataraman, C. Nuckolls, *Nat. Rev. Mater.* **2016**, *1*, 16002; e)A. C. Aragonès, N. L. Haworth, N. Darwish, S. Ciampi, N. J. Bloomfield, G. G. Wallace, I. Diez-Perez, M. L. Coote, *Nature* **2016**, *531*, 88-91; f)I. W. P. Chen, W.-H. Tseng, M.-W. Gu, L.-C. Su, C.-H. Hsu, W.-H. Chang, C.-h. Chen, *Angew. Chem. Int. Ed.* **2013**, *52*, 2449-2453.

[2] I. Ratera, J. Veciana, *Chem. Soc. Rev.* **2012**, *41*, 303-349.

[3] a)Y.-h. Zhang, S. Kahle, T. Herden, C. Stroh, M. Mayor, U. Schlickum, M. Ternes, P. Wahl, K. Kern, *Nat. Commun.* **2013**, *4*, 2110; b)R. Frisenda, R. Gaudenzi, C. Franco, M. Mas-Torrent, C. Rovira, J. Veciana, I. Alcon, S. T. Bromley, E. Burzurí, H. S. J. van der Zant, *Nano Lett.* **2015**, *15*, 3109-3114; c)J. Liu, H. Isshiki, K. Katoh, T. Morita, B. K. Breedlove, M. Yamashita, T. Komeda, *J. Am. Chem. Soc.* **2013**, *135*, 651-658; d)R. Request, S. Modesti, P. P. Baruselli, A. Smogunov, M. Fabrizio, E. Tosatti, *Proc. Nat. Acad. Sci. U.S.A.* **2014**, *111*, 69-74.

[4] J. P. Bergfield, G. C. Solomon, C. A. Stafford, M. A. Ratner, *Nano Lett.* **2011**, *11*, 2759-2764.

[5] a)C. Simão, M. Mas-Torrent, N. Crivillers, V. Lloveras, J. M. Artés, P. Gorostiza, J. Veciana, C. Rovira, *Nat. Chem.* **2011**, *3*, 359-364; b)R. Hayakawa, M. A. Karimi, J. Wolf, T. Huhn, M. S. Zöllner, C. Herrmann, E. Scheer, *Nano Lett.* **2016**, *16*, 4960-4967.

[6] L. Yuan, C. Franco, N. Crivillers, M. Mas-Torrent, L. Cao, C. S. S. Sangeeth, C. Rovira, J. Veciana, C. A. Nijhuis, *Nat. Commun.* **2016**, *7*, 12066.

[7] J. Karpinska, B. Starczewska, H. Puzanowska-Tarasiewicz, *Anal. Sci.* **1996**, *12*, 161-170.

[8] a)J. D. Bell, J. F. Blount, O. V. Briscoe, H. C. Freeman, *Chem. Commun,* **1968**, 1656-1657; b)T. Uchida, M. Ito, K. Kozawa, *Bull. Chem. Soc. Jpn.* **1983**, *56*, 577-582.

[9] a)R. Y. Lai, X. Kong, S. A. Jenekhe, A. J. Bard, *J. Am. Chem. Soc.* **2003**, *125*, 12631-12639; b)K. Wu, Y. Du, H. Tang, Z. Chen, T. Lian, *J. Am. Chem. Soc.* **2015**, *137*, 10224-10230; c)R. S. Nobuyasu, Z. J. Ren, G. C. Griffiths, A. S. Batsanov, P. Data, S. K. Yan, A. P. Monkman, M. R. Bryce, F. B. Dias, *Adv. Opt. Mater.* **2016**, *4*, 597-607.

[10] a)W. Hong, D. Z. Manrique, P. Moreno-García, M. Gulcur, A. Mishchenko, C. J. Lambert, M. R. Bryce, T. Wandlowski, *J. Am. Chem. Soc.* **2012**, *134*, 2292-2304; b)D. Z. Manrique, C. Huang, M. Baghernejad, X. Zhao, O. A. Al-Owaedi, H. Sadeghi, V. Kaliginedi, W. Hong, M. Gulcur, T. Wandlowski, M. R. Bryce, C. J. Lambert, *Nat. Commun.* **2015**, *6*, 6389; c)X. Liu, S. Sangtarash, D. Reber, D. Zhang, H. Sadeghi, J. Shi, Z.-Y. Xiao, W. Hong, C. J. Lambert, S.-X. Liu, *Angew. Chem. Int. Ed.* **2017**, *56*, 173-176; d)C. Huang, M. Jevric, A. Borges, S. T. Olsen, J. M. Hamill, J.-T. Zheng, Y. Yang, A. Rudnev, M. Baghernejad, P. Broekmann, A. U. Petersen, T. Wandlowski, K. V. Mikkelsen, G. C. Solomon, M. Brøndsted Nielsen, W. Hong, *Nat. Commun.* **2017**, *8*, 15436.

[11] P. Moreno-García, M. Gulcur, D. Z. Manrique, T. Pope, W. Hong, V. Kaliginedi, C. Huang, A. S. Batsanov, M. R. Bryce, C. Lambert, T. Wandlowski, *J. Am. Chem. Soc.* **2013**, *135*, 12228-12240.

[12] a)D. Clarke, B. C. Gilbert, P. Hanson, C. M. Kirk, *J. Chem. Soc., Perkin Trans. 2* **1978**, 1103-1110; b)T. Okamoto, M. Kuratsu, M. Kozaki, K. Hirotsu, A. Ichimura, T. Matsushita, K. Okada, *Org. Lett.* **2004**, *6*, 3493-3496; c)Y. Gao, J. Chen, X. Zhuang, J. Wang, Y. Pan, L. Zhang, S. Yu, *Chem. Phys.* **2007**, *334*, 224-231; d)H. J. Shine, E. E. Mach, *J. Org. Chem.* **1965**, *30*, 2130-2139.

[13] R. E. Hester, K. P. J. Williams, *J. Chem. Soc., Perkin Trans. 2* **1981**, 852-859.

[14] a)C. Lagercrantz, *Acta Chem. Scand.* **1961**, *15*, 1545-1556; b)Y. Soo Kang, J. A. Jung, L. Kevan, *J. Chem. Soc., Faraday Trans.* **1998**, *94*, 3247-3250; c)F. L. Rupérez, J. C. Conesa, J. Soria, *Spectrochim. Acta, Part A* **1984**, *40*, 1021-1024.

[15] W. Hong, H. Valkenier, G. Mészáros, D. Z. Manrique, A. Mishchenko, A. Putz, P. M. García, C. J. Lambert, J. C. Hummelen, T. Wandlowski, *Beilstein J. Nanotechnol.* **2011**, *2*, 699-713.

[16] a)V. Fatemi, M. Kamenetska, J. B. Neaton, L. Venkataraman, *Nano Lett.* **2011**, *11*, 1988-1992; b)B. Capozzi, J. Xia, O. Adak, E. J. Dell, Z.-F. Liu, J. C. Taylor, J. B. Neaton, L. M. Campos, L. Venkataraman, *Nat. Nanotechnol.* **2015**, *10*, 522-527.

[17] a)V. Kaliginedi, P. Moreno-García, H. Valkenier, W. Hong, V. M. García-Suárez, P. Buiter, J. L. H. Otten, J. C. Hummelen, C. J. Lambert, T. Wandlowski, *J. Am. Chem. Soc.* **2012**, *134*, 5262-5275; b)R. Frisenda, S. Tarkuç, E. Galán, M. L. Perrin, R. Eelkema, F. C. Grozema, H. S. J. van der Zant, *Beilstein J. Nanotechnol.* **2015**, *6*, 1558-1567.

[18] K. Yoshida, I. V. Pobelov, D. Z. Manrique, T. Pope, G. Mészáros, M. Gulcur, M. R. Bryce, C. J. Lambert, T. Wandlowski, *Sci. Rep.* **2015**, *5*, 9002.

[19] a)C. A. Martin, D. Ding, J. K. Sørensen, T. Bjørnholm, J. M. van Ruitenbeek, H. S. J. van der Zant, *J. Am. Chem. Soc.* **2008**, *130*, 13198-13199; b)S. Y. Quek, M. Kamenetska, M. L. Steigerwald, H. J. Choi, S. G. Louie, M. S. Hybertsen, J. B. Neaton, L. Venkataraman, *Nat. Nanotechnol.* **2009**, *4*, 230-234.

[20] a)B. Gotsmann, H. Riel, E. Lörtscher, *Phys. Rev. B* **2011**, *84*, 205408; b)R. Quan, C. S. Pitler, M. A. Ratner, M. G. Reuter, *ACS Nano* **2015**, *9*, 7704-7713.

[21] a)C. Untiedt, A. Yanson, R. Grande, G. Rubio-Bollinger, N. Agraït, S. Vieira, J. M. van Ruitenbeek, *Phys. Rev. B* **2002**, *66*, 085418; b)M. Kamenetska, S. Y. Quek, A. C. Whalley, M. L. Steigerwald, H. J. Choi, S. G. Louie, C. Nuckolls, M. S. Hybertsen, J. B. Neaton, L. Venkataraman, *J. Am. Chem. Soc.* **2010**, *132*, 6817-6821.

[22] D. Pan, D. L. Phillips, *J. Phys. Chem. A* **1999**, *103*, 4737-4743.

[23] a)M. S. José, A. Emilio, D. G. Julian, G. Alberto, J. Javier, O. Pablo, S.-P. Daniel, *J. Phys-Condens. Mat.* **2002**, *14*, 2745; b)A. R. Rocha, V. M. Garcia-suarez, S. W. Bailey, C. J. Lambert, J. Ferrer, S. Sanvito, *Nat. Mater.* **2005**, *4*, 335-339.

[24] J. Ferrer, C. J. Lambert, V. M. García-Suárez, D. Z. Manrique, D. Visontai, L. Oroszlany, R. Rodríguez-Ferradás, I. Grace, S. W. D. Bailey, K. Gillemot, S. Hatef, L. A. Algharagholy, *New J. Phys.* **2014**, *16*, 093029.

[25] S. Choi, B. Kim, C. D. Frisbie, *Science* **2008**, *320*, 1482-1486.

[26] a)H. Song, Y. Kim, Y. H. Jang, H. Jeong, M. A. Reed, T. Lee, *Nature* **2009**, *462*, 1039-1043; b)P. Reddy, S.-Y. Jang, R. A. Segalman, A. Majumdar, *Science* **2007**, *315*, 1568-1571.

[27] a)C. J. Lambert, *Chem. Soc. Rev.* **2015**, *44*, 875-888; b)R. Frisenda, V. A. E. C. Janssen, F. C. Grozema, H. S. J. van der Zant, N. Renaud, *Nat. Chem.* **2016**, *8*, 1099-1104; c)A. Mishchenko, L. A. Zotti, D. Vonlanthen, M. Bürkle, F. Pauly, J. C. Cuevas, M. Mayor, T. Wandlowski, *J. Am. Chem. Soc.* **2011**, *133*, 184-187; d)G. Kastlunger, R. Stadler, *Phys. Rev. B* **2013**, *88*, 035418.

COMMUNICATION
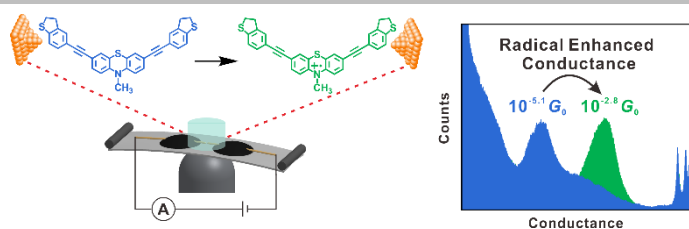
Single-molecule conductances of phenothiazine radicals have been measured using Mechanically Controllable Break Junction technique. Triggered by acid oxidant, the radical cation of phenothiazine enhances the charge transport property by up to 200 times with high stability and high junction formation probability at room-temperature, which leads to promising applications in single-molecule electronics and spintronics.

Junyang Liu, Xiaotao Zhao, Qusiy Al-Galiby, Xiaoyan Huang, Jueting Zheng, Ruihao Li, Cancan Huang, Yang Yang, Jia Shi, David Manrique, Colin Lambert*, Martin R. Bryce*, Wenjing Hong*

Radical Enhanced Charge Transport of Single-Molecule Phenothiazine Electrical Junctions

Supporting Information

Radical Enhanced Charge Transport in Single-Molecule Phenothiazine Electrical Junctions

Junyang Liu[#], Xiaotao Zhao[#], Qusiy Al-Galiby[#], Xiaoyan Huang, Jueting Zheng, Ruihao Li, Cancan Huang, Yang Yang, Jia Shi, David Zsolt Manrique, Colin Lambert*, Martin R. Bryce*, Wenjing Hong*

Supporting Information

Content:

1. Synthesis and chemical analysis of molecule 10-Methyl-PTZ.
2. Conductance measurements by MCBJ technique.
3. Blank experiment results for pure solvent and with TFA addition.
4. OPE molecule measurements before and after TFA addition.
5. Long-term stability test by single-molecule conductance measurements and UV-Vis spectroscopy.
6. Theoretical calculation methods.
7. Corrections to DFT

1. Synthesis and chemical analysis of molecule 10-Methyl-PTZ.

1-1. Synthesis of molecule **PTZ-BT** is shown in Scheme S1.

A   **PTZ-BT**   **Scheme S1.**
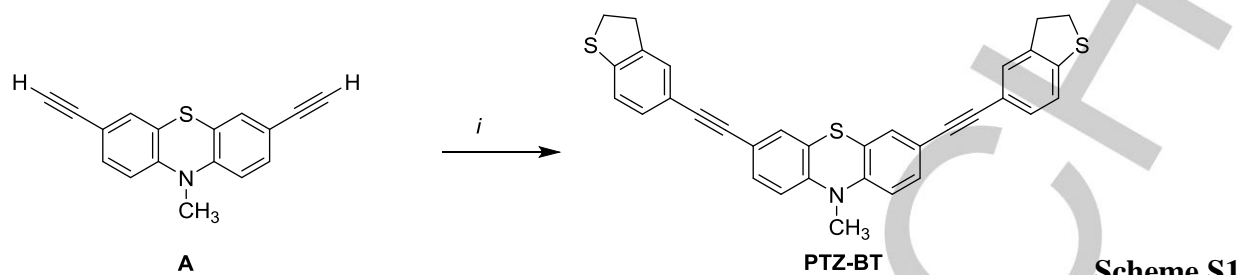
Reagents and conditions: *i)* 2,3-Dihydro-5-iodobenzo[*b*]thiophene, Pd(PPh$_3$)$_4$, CuI, THF/Et$_3$N, 20 h, rt, 60%.

    Synthesis of molecule **PTZ-BT**. To a solution of **A**[1] (80 mg, 0.3 mmol), Pd(PPh$_3$)$_4$ (35 mg, 0.03 mmol) and CuI (6 mg, 0.03 mmol) in THF/Et$_3$N (3:1 *v/v*) (10 ml), 2,3-dihydro-5-iodobenzo[*b*]thiophene[2] (200mg, 0.75mmol) was added. The mixture was stirred for 20 h at r.t. and solvent was removed by vacuum evaporation. Purification by column chromatography gave a yellow solid (95 mg, 60% yield). mp: decomp. >265 ^{o}C.

^{1}H NMR (700 MHz, CD$_2$Cl$_2$) δ 7.32 (m, 4H), 7.25 (m, 4H), 7.17 (d, *J* = 7.9 Hz, 2H), 6.80 (d, *J* = 7.9 Hz, 2H), 3.39 (m, 7H), 3.29 (t, *J* = 8.1 Hz, 4H).

^{13}C NMR (176 MHz, CD$_2$Cl$_2$) δ 145.06, 142.64, 140.66, 130.88, 130.44, 129.52, 126.97, 122.78, 121.75, 118.69, 117.59, 114.11, 89.49, 87.8, 35.82, 35.38, 33.40.

HR-MS (ASAP+) *m/z* calcd for C$_{33}$H$_{23}$NS$_3$ [M]$^+$ 529.0978, found *m/z*: [M]$^+$ 529.0993. Anal. Calcd. for C$_{33}$H$_{23}$NS$_3$: C, 74.82; H, 4.38; N, 2.64. Found: C, 75.02; H, 4.54; N, 2.68.

1-2. NMR spectra
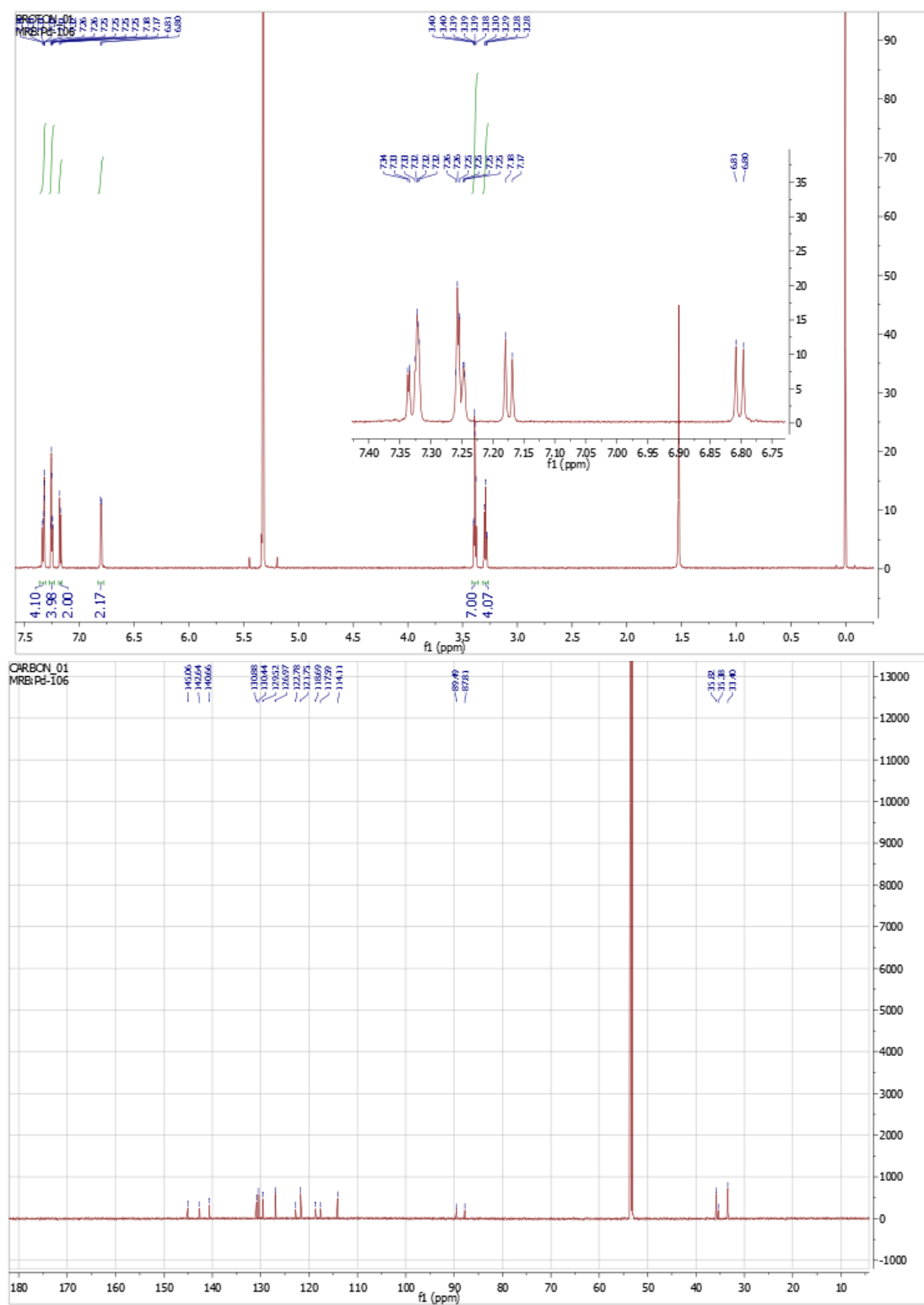
Figure S1. ^{1}H NMR and ^{13}C NMR spectra of molecule **PTZ-BT** in CD_2Cl_2.

2. Conductance measurements by MCBJ technique

For MCBJ experiments, nanogaps were fabricated between a notched, suspended gold wire (0.1 mm diameter, 99.99%, Jiaming, Beijing) fixed onto a spring steel sheet (10 mm×30 mm, thickness 0.20 mm) by a two-component epoxy glue (Stycast 2850 FT with catalyst 9). A polytef liquid cell containing solution of target molecule sealed by a plastic O-ring (FFKM 6.07*1.78, Wuxi Bo Yate Sealing Technology Development Co. Ltd.), which is to prevent liquid leakage, was mounted onto the sheet as shown in Figure S2b. During the measurements, the sample sheet is bent with a pushing rod, which is driven by a combination of a stepping motor (Zaber NA14B16 linear actuator) and a piezo stack (Thorlab AE0505D18F). The setup is shown in Figure S2. By applying a DC voltage of 100 mV, the current passing through electrode pairs was measured by a lab-built logarithm *I-V* converter with a sampling rate of 100 *k*Hz using National Instrument CompactRIO-9073 for data acquisition. This converter outputs the sampling voltage by signal amplification for 1 *f*A to ~1 mV, and the background noise level is ~10 mV that the current measuring sensitivity is at the range of ~10 *f*A.

The single-molecule conductance measurements were carried out at room temperature in solution containing 0.1 mM of target molecule in a mixture of tetrahydrofuran (THF, Sigma-Aldrich, p.a) and 1,3,5-trimethylbenzene (TMB, Aldrich, p.a.), 1:4 (*v/v*). Since THF and TMB are polar and non-polar solvents, respectively. The polar THF will increase the leakage current and therefore increase the noise level, and the non-polar TMB helps to lower the conductance background. However, most of the molecules investigated need the polar solvent to enhance their solubility, therefore, THF can be used to dissolve most of the molecules, and TMB is used to decrease the leakage current. After screening the optimal ratio of the THF/TMB mixture, we found that 1:4 *v/v* is optimum for single-molecule conductance measurements, as shown for a range of other molecules in our previous publications[3] and also by Dr. Michel Calame's group in Basel University.[4]

We apply the same tapping condition including the electrode stretching rate of about 50 nm/s, and also the same logarithm *I-V* convertor for the single-molecule conductance measurements of the **PTZ-BT** and **PTZ-BT+•**. The difference in the noise levels between the neutral and radical molecules is mainly due to the large ion concentration induced by the addition of TFA. After the breaking of the molecular junction, the conductance trace of **PTZ-BT+•** falls to a relatively higher background of about $10^{-5.5}$ G_0 compared to 10^{-8} G_0 of **PTZ-BT**. Since the noise levels in both measurements are lower than the molecular conductance, the difference in the noise level will not influence the break junction measurement. Further technical details of the MCBJ experiment are given in our previous reports.[3a, 3b]
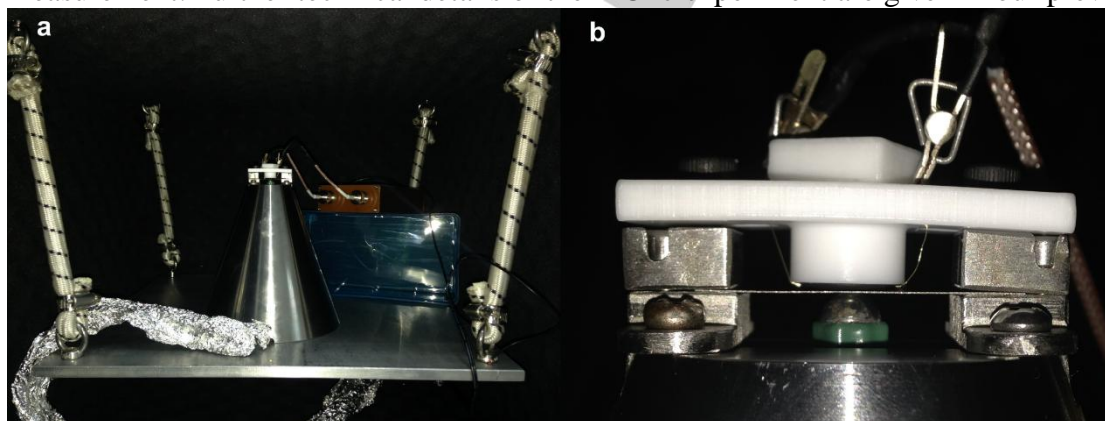

Figure S2. The Mechanically Controllable Break Junction setup for (a) the whole view and (b) the enlarged view of chip with liquid cell.

3. Blank experiment results for pure solvent and with TFA addition.

We also calibrated the stretching rate of gold electrodes using a previous method.[3b] We used the pure THF:TMB (*v/v* 1:4) solvent without target molecule as a blank experiment for the calibration of

distance for MCBJ experiments. The 1D conductance histogram and 2D conductance-distance histogram in Figure S3(a) and S3(b) show direct tunneling and clear non-plateau features, suggesting a pure and clean environment inside the gap. According to the measured tunneling decay constant ($\log[\Delta G/G_0]/\Delta z = -5.5$ nm^{-1}) in the same solvent using STM-BJ technique,[3a] we calibrate the relative displacement in the conductance range from 10^{-4} to 10^{-6} G_0 to be ~0.36 nm (-2/-5.5 = ~0.36 nm), as shown in the inset of Figure S3(a).

Furthermore, the snap-back distance has also been calculated.[3b] Since a perfect linear atomic chain of gold has a conductance of G_0, we assume that $\log(G/G_0) = -\alpha z$, where $z = 0$ corresponds to the point where the distance between the terminating gold atoms is equal to the equilibrium gold-gold separation. As the measured separation $\Delta z = z - z_{corr}$, where z_{corr} is the snap-back distance, a plot of $\log(G/G_0)$ versus Δz has a slope of $-\alpha$ and an intercept of αz_{corr}. The electrode stretching rate has been calibrated by measuring the conductance G versus Δz ranging from 10^{-4} to 10^{-6} G_0 to extract the slope and the intercept. From the repeated measurements, we obtained a displacement distribution of the intercepts extended from the range of 10^{-4} G_0 to 10^{-6} G_0 to a range of $10^{-0.3}$ G_0 to $10^{-6.0}$ G_0, which the $10^{-0.3}$ G_0 is the zero set point of the conductance-distance curve, the most probable displacement was found to be 0.5 nm, in agreement with our previous studies.[3b] This is the snap-back distance previously calibrated in the gold electrodes system, (as shown in the inset of Figure S3(b)).

In order to confirm that the conductance signal of the **PTZ-BT+•** did not come from TFA, we also did the control experiment to measure the solution of 20% TFA in the mixed THF:TMB solution. The blank experiment exhibited a non-peak feature, indicating that the TFA would not affect the conductance measurements for PTZ molecules. Since the background is above $10^{-6.0}$ G_0 due to the high ionic concentration, the conductance range from 10^{-3} to 10^{-4} G_0 was selected to calibrate the relative displacement (-1/-5.5 = ~0.18 nm), therefore, the most probable displacement from $10^{-0.3}$ G_0 to $10^{-4.0}$ G_0 was also found to be 0.18 nm due to the fast snap-back above $10^{-3.0}$ G_0, as shown in the upper inset in the Figure S3d.
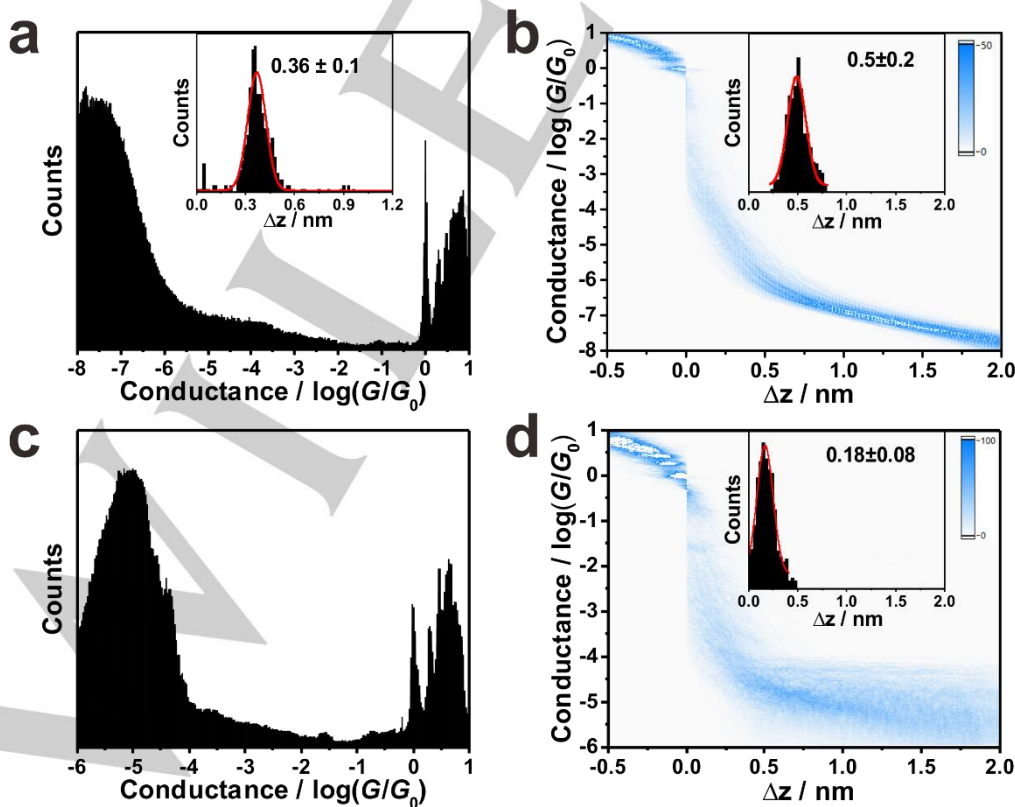
Figure S3. (a) 1D conductance histogram and (b) conductance-distance histogram for the mixed solvent of THF:TMB (*v/v* 1:4), the inset of (a) shows the relative displacement distribution determined from $10^{-4.0}$ G_0 to $10^{-6.0}$ G_0 for the calibration of the stretching rate of the electrodes pair, the inset of (b) shows the snap-back distance determined from $10^{-0.3}$ G_0 to $10^{-6.0}$ G_0. (c) 1D conductance histogram and (d) conductance-distance histogram for 20% TFA in the mixed solvent of THF:TMB (*v/v* 1:4), the upper inset shows the relative displacement distribution from $10^{-0.3}$ G_0 to $10^{-4.0}$ G_0.

4. OPE molecule measurements before and after TFA addition.

In order to exclude the possible solvent tuning effect during the conductance measurements,[5] the control experiment of some molecules which will not react with TFA should be conducted. Here we use the tolane derivative OPE2-BT which was previously reported,[2] and the measured results are showed in Figure S4. The same 20% volume ratio of TFA added into the mixed THF/TMB solvent will actually affect the single-molecule charge transport due to the polarizability change of the solvent, however, the conductance only increases from $10^{-2.98}$ G_0 to $10^{-2.88}$ G_0, which means 1.26 times enhancement. This is much lower than that of 200 times when the radical cation state is triggered in the PTZ system. Therefore, the conductance enhancement in the main text for the PTZ system mainly originates from the radical state instead of the solvent tuning effect.
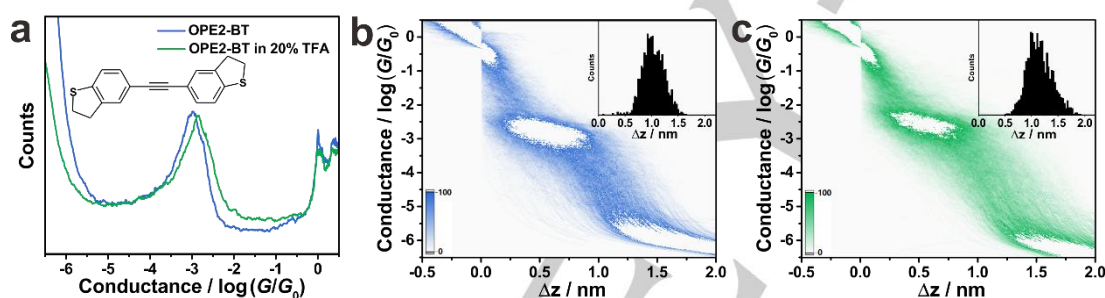

Figure S4. (a) Conductance histogram comparison between the OPE2-BT molecule before and after the TFA addition. The conductance-distance histogram (b) before and (c) after the TFA addition, the relative displacement distribution histogram is shown in upright inset of each state.

5. Radical stability test by UV-Vis spectroscopy

5-1. The conductance measurement of **PTZ-BT+•** after two months.

The solution of **PTZ-BT+•** stored two months was added into the liquid cell for conductance measurement again to test the long-term stability. As shown in Figure S5-1, the statistical results for 2000 traces suggests that the conductance peak remains at $10^{-2.8}$ G_0, with the same distribution of conductance relative displacement, which suggests the long-term stability of the radical cation. Therefore, this conductance result is added into Figure 4 in the main text for better comparison.
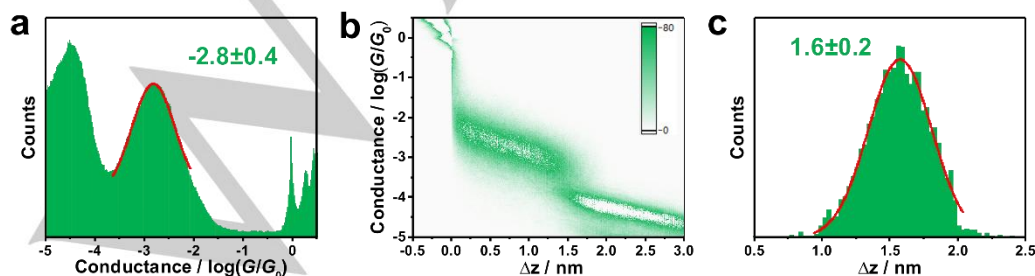
Figure S5-1. The conductance measurement results of (a) the conductance histogram, (b) the conductance-distance histogram and (c) the relative displacement distribution of **PTZ-BT+•** after two months.

5-2. The UV-Vis measurement of **PTZ-BT+•** after two months.

   To further confirm the stability of the radical cation, the solution of **PTZ-BT+•** which was used for conductance measurements in Figure 4 in the main text was also used for the UV-Vis spectroscopy. Figure S5-2 shows the obtained UV-Vis spectra after two days and even after two months' storage at room temperature. Compared with those at the initial time of TFA addition, although the intensity of the absorption peak around 518 nm is lowered, the peak position was still almost the same. Therefore, accompanying the conductance stability test of Figure 4, the spectroscopic stability confirmed that the radical cation of phenothiazine can last at least two months at room temperature.
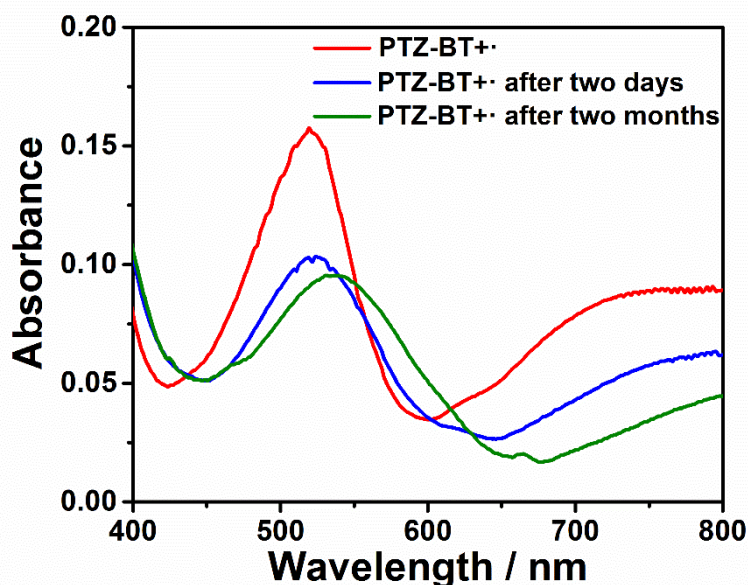

Figure S5-2. The UV-Vis spectra of **PTZ-BT+•** after two days and two months.

6. Theoretical calculation methods

6-1. Theoretical estimation of molecular length and dihedral angle
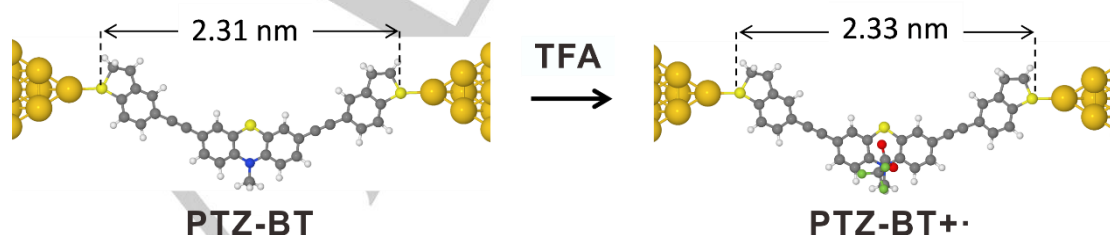

Figure S6-1 The molecular length calculations of relaxed geometries for two states, **PTZ-BT** and **PTZ-BT+•**.

   Figure S6-1 shows the molecular length calculation of relaxed geometries for two states, namely, **PTZ-BT** and **PTZ-BT+•**. The simulations were carried out by firstly geometrically optimizing the isolated **PTZ-BT** molecule. Then the TFA molecule was placed near the central N-atom of the **PTZ-BT**

molecule, and the combined structure was relaxed again (See for example in the Figure S6-1b the **PTZ-BT+•** structure). The relaxed geometry was found using the density functional (DFT) code SIESTA,[6] which employs Troullier-Martins pseudopotentials to represent the potentials of the atomic cores,[7] and a local atomic-orbital basis set. We used double zeta polarized basis set for all atoms and the generalized gradient approximation with Perdew-Burke-Ernzerhof functional (GGA-PBE) for the exchange and correlation for the geometrical optimization.[8] After the geometry relaxation of the combined structure of TFA and **PTZ-BT** (referred as **PTZ-BT+•)**, the distance (D), the number of electrons transferred (ΔN) and the binding energy (E_b) between the PTZ core and TFA were computed, which is shown in Table S6-1. The calculation shows that at the distance 2.73 Å the PTZ molecule lost approximately one electron and formed the radical cation **PTZ-BT+•**. The calculation did not find significant geometrical changes to **PTZ-BT** but a slight increase in molecular length from 2.31 nm of **PTZ-BT** to 2.33 nm of **PTZ-BT+•** due to the TFA, as Figure S6-1 illustrates. The various angles in the **PTZ-BT** and **PTZ-BT+•** are illustrated in Figure S6-2. The angles within the **PTZ-BT** molecule changed due to the presence of the TFA such that the PTZ core has become slightly more planar, in agreement with previous studies (Refs 8b, 22 in the main text). We have found that the radical cation has a slightly more planar molecular structure, with the S-S-S angle of PTZ core increasing approximately from 147.5° for **PTZ-BT** to 149.6° for **PTZ-BT+•** (Figure S6-1c)

Table S6-1: Number of electrons (ΔN) transferred from the PTZ molecule to the TFA, and the distance (D), the binding energy (E_b) between the PTZ core and TFA. The right-most column shows the number of electrons ($-\Delta N_{SR}$) transferred from the scattering region (SR) comprising the TFA and each electrode tip. (Each tip consists of 4 gold atoms.) All charges are obtained from the Mulliken populations computed by SIESTA.

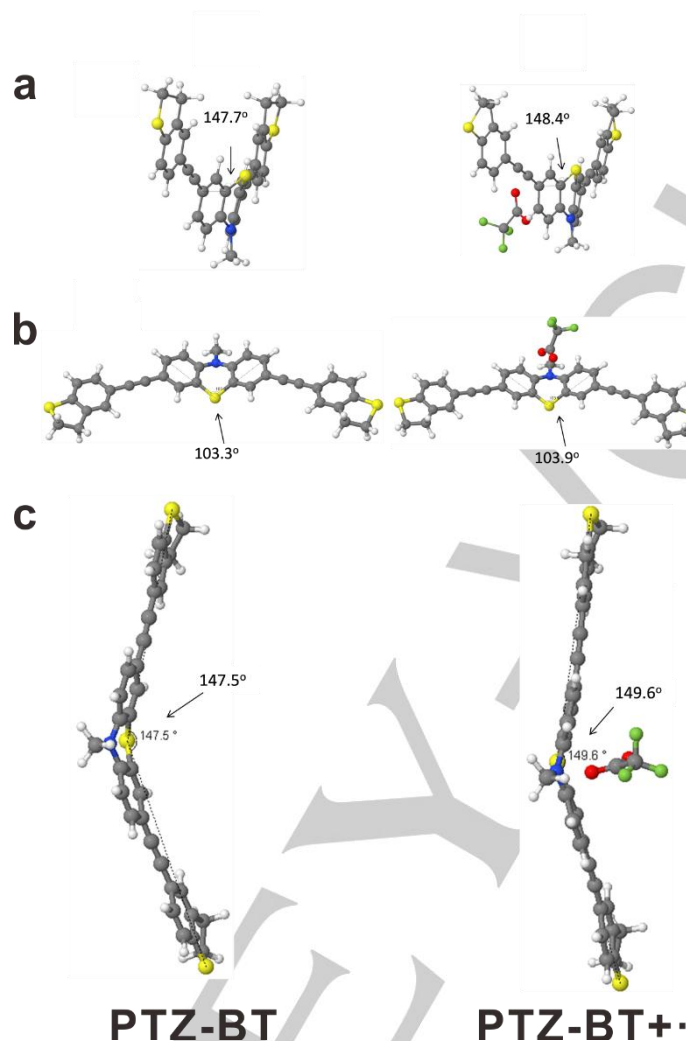| State	$-\Delta N$ (elec.)	D (Å)	E_b (eV)	$-\Delta N_{SR}$
PTZ-BT+•	0.758	2.73	-0.863	0.979

Figure S6-2 (a), (b), (c) shows the DFT calculated C-C-S, C-S-C and S-S-S angles, respectively of relaxed geometries for two states, **PTZ-BT** and **PTZ-BT+•** ((a), (b) and (c) show the same geometric structures with different point views). Due to the TFA, the core dihedral angles increase slightly, leading to the more flattened PTZ core.

6-2. Geometry, transmission and conductance calculations

After obtaining the relaxed geometries of the **PTZ-BT** and the **PTZ-BT+•** structures, they were placed between gold electrodes as shown Figure S6-1 and the geometries were further optimized using the SIESTA code, as described above. The initial distance between the center of the S atom and the center of the apex atom of each gold pyramid was 2.5 Å. After geometry optimization, the distance changed to a final value of 2.61 Å. Figure S6-1 shows the central region of the junction, that is composed of a single molecule attached to two gold leads in (111) direction. In order to calculate electronic transport through the molecule from the left electrode to the right electrode we used GOLLUM.[9] GOLLUM is a next-generation code, born out of the SMEAGOL code [10] and uses the spin-dependent Hamiltonian obtained from density functional theory to compute transport properties of a wide variety of nanostructures. The Hamiltonian and overlap matrices are also calculated with SIESTA using DZP basis sets for all elements except gold, for which DZ basis set was used, GGA-PBE exchange-correlation parameterization, 0.0001 density-matrix tolerance and 200Ry grid cutoff. The Mulliken charges are computed consistently with the same setup, showing the charge transfer between

the **PTZ-BT** and TFA and the formation of **PTZ-BT+•**. In the quantum transport simulation, we used a spin polarized Hamiltonian to investigate the electron and spin transport properties of the system. For each spin σ, we used the GOLLUM quantum transport code[9] to compute the transmission coefficient $T^{\sigma}(E)$ for electrons of energy E passing from the left gold electrode to the right electrode. Once $T^{\sigma}(E)$ is computed, we calculated the zero-bias electrical conductance G using the finite temperature Landauer formula:

$$G = (G^{\uparrow} + G^{\downarrow})/2 \qquad (1)$$

$$G^{\sigma} = G_0 \int_{-\infty}^{\infty} dE \, T^{\sigma}(E) \left(-\frac{df(E)}{dE} \right) \qquad (2)$$

where $G_0 = \left(\frac{2e^2}{h} \right)$ is the quantum of conductance, and $f(E,T)$ is Fermi distribution function defined as $f(E,T) = [e^{(E-E_F)/k_B T} + 1]^{-1}$ with T = 300 K room temperature, where k_B is Boltzmann's constant. In case of spin-polarized calculation $T^{\sigma}(E)$ is the transmission coefficient for electrons of energy E, spin σ = [↑, ↓] passing through the molecule from one electrode to the other.

When the TFA is placed close to the **PTZ-BT** molecule, the **PTZ-BT** loses approximately one electron. Figures S6-3a, b show the spin-dependent and total transmission coefficients of the two states **PTZ-BT** and **PTZ-BT+•**. The **PTZ-BT** (left) and **PTZ-BT+•** (right) relative to the DFT-predicted Fermi energy E_F^{DFT}. Figure 3 in the main text shows the averaged transmission coefficients as well as the room temperature conductance calculated from the transmission coefficients.
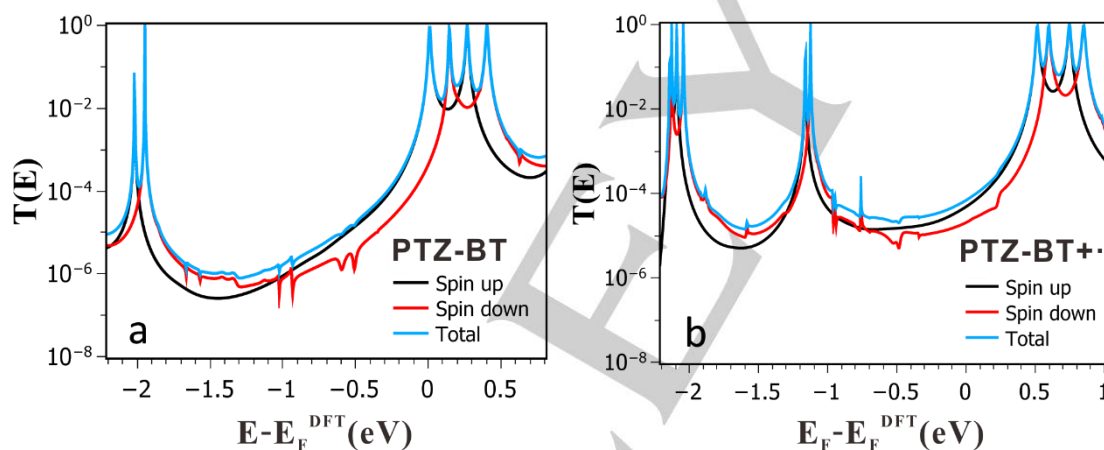

Figure S6-3. (a and b) show the spin-dependent and total transmission coefficients as a function of energy for two states, **PTZ-BT** and **PTZ-BT+•**.

After adding TFA, the radial cation is formed and the TFA acts like a negatively charged gate, which increases the HOMO and LUMO energies of **PTZ-BT+•** relative to those of **PTZ-BT**. To illustrate the origin of sharp features at E=-1.2 (green curve) in Figure 3 in the main text, and E=-2 (blue curve) in Figure S6-3b, we plotted the frontier molecular orbitals of the PTZ molecule in the **PTZ-BT** and **PTZ-BT+•** states as shown in Figure S6-4 and Figure S6-5, respectively. Figure S6-5 shows the frontier molecular orbitals of the HOMO of **PTZ-BT+•** are delocalized across their central backbones. However, the charge distribution of the HOMO is different from that of the LUMO and therefore their energies shift by different amounts in response to the repulsive interaction with the TFA. In addition, as shown by the binding energy between the **PTZ** core and TFA in Table S6-1 in SI, the TFA is chemisorbed to the **PTZ**, which causes a further differential shift in the frontier orbitals. Since the experimental voltages are 100 mV, which are relatively low, all traces are calculated at zero bias. The calculations showed a rather smaller HOMO-LUMO gap of the **PTZ-BT+•** (about 1.6 eV) than that of **PTZ-BT** (about 2 eV),

and exhibited higher transmittance for **PTZ-BT+•** due to the Fermi energy shift, which is also confirmed by the red-shift of the UV-Vis spectra from Figure 1a in the manuscript. Besides, since the charge transport of BT anchors are always dominated by the HOMO, it suggests that the Fermi level is closer to the HOMO energy of **PTZ-BT+•**, thus exhibiting higher conductance, which follows the same trend as the experiments.
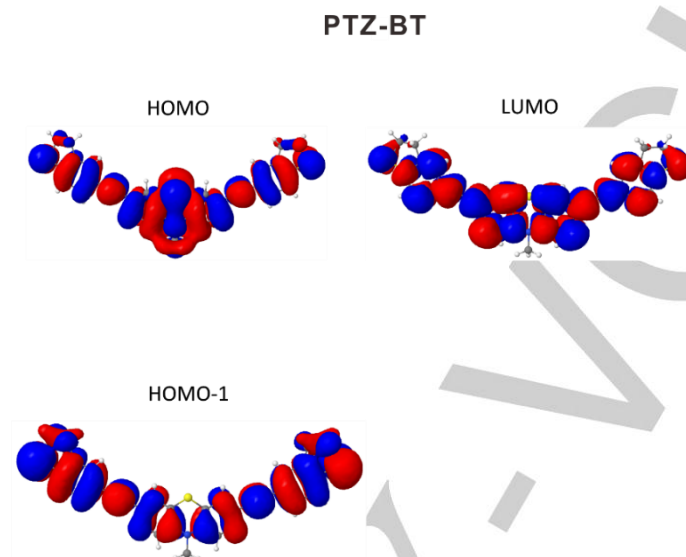

Figure S6-4: Frontier molecular orbitals of the PTZ molecule in the state **PTZ-BT** obtained using the DFT code SIESTA. Red corresponds to positive and blue to negative regions of the wave functions.
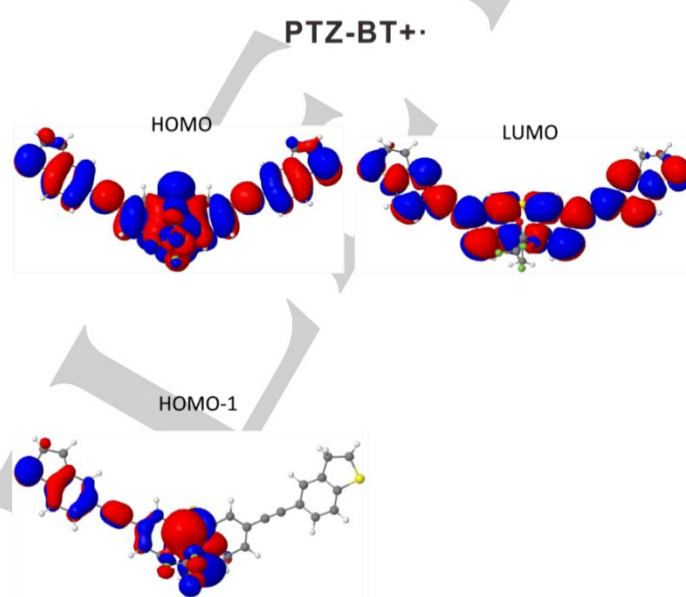

Figure S6-5: Frontier molecular orbitals of the PTZ molecule in the state **PTZ-BT+•** obtained using the DFT code SIESTA. Red corresponds to positive and blue to negative regions of the wave functions.

7. Corrections to DFT

DFT has problems with the issue of Fermi level alignment, the underestimation of the HOMO-LUMO gap and (related or unrelated) self-interaction which decreases charge localization artificially. More accurate methods such as GW come with their own sets of technical difficulties such as

prohibitive demands on computational resources. Therefore, ad-hoc corrections are needed when DFT calculations are compared with experimental measurements. Some groups use scissor-operator corrections for that purpose, others use atomic self-interaction corrections. In our case, we take advantage of the availability of experimental data by shifting E_F such that $T(E_F)$ fits the experimental conductance, to within a constant of proportionality. This approach has been quite successful in previous joint papers with other experimentalists.[3c, 11]

The need to correct DFT in this manner is widely recognized. The deficiencies of DFT has been described in our review article,[12] and has shown that for simple molecules, some of these deficiencies can be overcome using GW theory[13] or quantum Monte Carlo methods[14]. However, for complicated structures such as those considered here, these methods are not tractable and DFT is the only realistic approach. We know that DFT can predict trends in homologous series of molecular wires, as well as changes due to electrostatic, electrochemical or mechanical gating. However, DFT struggles to predict actual conductance values, because small changes in the charge on a molecule can produce significant shifts the HOMO and LUMO energies. As noted in the article[15], *"The correct description of localized charges is notoriously hard to achieve within a DFT framework because the Coulomb and exchange parts of the interaction of an electron with itself do not cancel out exactly in a standard Kohn-Sham (KS) Hamiltonian and the corresponding self-interaction (SI) errors result in an artificial tendency towards delocalization."* When making comparisons with experiment, theory also struggles to locate the value of the Fermi energy of the experimental electrodes relative to the frontier orbitals of the molecule, because screening by the electrodes depends on the shape of the electrodes. The latter is an unknown quantity, which varies from measurement to measurement and also depends on the contacting technique employed.

One example illustrating the need for corrections is ref[11]. Figure 2 of that paper shows that the DFT-predicted conductance values are two orders of magnitude too high. Clearly a correction to the DFT-predicted Fermi energy would yield closer agreement with experiment by moving the Fermi energy closer to the HOMO-LUMO gap. Agreement would be further improved by implementing a scissor correction, which increases the HOMO-LUMO gap. Although neither of these corrections is implemented, the DFT theory does have its value, because it predicts the correct trends. Similarly, in our case, as shown in Figure 3 of our manuscript, when the TFA was placed near the core of **PTZ-BT**, DFT correctly predicts the formation of the radical cation **PTZ-BT+•**, which is central to the theme of the paper.

Another example showing that corrections to DFT are needed, is the paper by the Columbia group[16], where DFT predicts that E_F lies close to the LUMO leading to predicted conductances, which again are orders of magnitude greater than the experimental values. In that paper it is stated "*A self-energy correction, including electrode polarization effects on the molecular orbital (MO) energy levels in the junction, was then added to the Hamiltonian,....*", which again has the effect of shifting the Fermi energy and adjusting the HOMO-LUMO gap.

In addition to the above corrections, one could also consider the role of the solvent, as discussed in ref[15], where it was found that a polar solvent stabilizes localized charges and can contribute to the transport Hamiltonian, thereby creating a transmission baseline. This increases the predicted conductance compared with a less expensive generalized ΔSCF method, which ignores the solvent and artificially fixes the charge on the counterion. Nevertheless, both approaches confirm the main trend that the electrical conductance in the charged state should be significantly higher than that of the neutral state. Ref[15] also concluded that some part of the charge should be absorbed by the leads, but most of it remains on the complex due to Coulomb attraction, where the vicinity of the localized charge on the

counterion has a stabilizing effect. In our case, this sharing of the charge is illustrated by Table S6-1, where the right-most column reveals that part of the charge resides on the electrode tips.

References for SI

[1] C. S. Krämer, K. Zeitler, T. J. J. Müller, *Org. Lett.* **2000**, *2*, 3723-3726.

[2] P. Moreno-García, M. Gulcur, D. Z. Manrique, T. Pope, W. Hong, V. Kaliginedi, C. Huang, A. S. Batsanov, M. R. Bryce, C. Lambert, T. Wandlowski, *J. Am. Chem. Soc.* **2013**, *135*, 12228-12240.

[3] a)W. Hong, H. Valkenier, G. Mészáros, D. Z. Manrique, A. Mishchenko, A. Putz, P. M. García, C. J. Lambert, J. C. Hummelen, T. Wandlowski, *Beilstein J. Nanotechnol.* **2011**, *2*, 699-713; b)W. Hong, D. Z. Manrique, P. Moreno-García, M. Gulcur, A. Mishchenko, C. J. Lambert, M. R. Bryce, T. Wandlowski, *J. Am. Chem. Soc.* **2012**, *134*, 2292-2304; c)D. Z. Manrique, C. Huang, M. Baghernejad, X. Zhao, O. A. Al-Owaedi, H. Sadeghi, V. Kaliginedi, W. Hong, M. Gulcur, T. Wandlowski, M. R. Bryce, C. J. Lambert, *Nat. Commun.* **2015**, *6*, 6389.

[4] S. Wu, M. T. Gonzalez, R. Huber, S. Grunder, M. Mayor, C. Schonenberger, M. Calame, *Nat. Nanotechnol.* **2008**, *3*, 569-574.

[5] a)V. Fatemi, M. Kamenetska, J. B. Neaton, L. Venkataraman, *Nano Lett.* **2011**, *11*, 1988-1992; b)B. Capozzi, J. Xia, O. Adak, E. J. Dell, Z.-F. Liu, J. C. Taylor, J. B. Neaton, L. M. Campos, L. Venkataraman, *Nat. Nanotechnol.* **2015**, *10*, 522-527.

[6] M. S. José, A. Emilio, D. G. Julian, G. Alberto, J. Javier, O. Pablo, S.-P. Daniel, *J. Phys-Condens. Mat.* **2002**, *14*, 2745.

[7] N. Troullier, J. L. Martins, *Phys. Rev. B* **1991**, *43*, 1993-2006.

[8] J. P. Perdew, K. Burke, M. Ernzerhof, *Phys. Rev. Lett.* **1996**, *77*, 3865-3868.

[9] J. Ferrer, C. J. Lambert, V. M. García-Suárez, D. Z. Manrique, D. Visontai, L. Oroszlany, R. Rodríguez-Ferradás, I. Grace, S. W. D. Bailey, K. Gillemot, S. Hatef, L. A. Algharagholy, *New J. Phys.* **2014**, *16*, 093029.

[10] A. R. Rocha, V. M. Garcia-suarez, S. W. Bailey, C. J. Lambert, J. Ferrer, S. Sanvito, *Nat. Mater.* **2005**, *4*, 335-339.

[11] A. Mishchenko, L. A. Zotti, D. Vonlanthen, M. Bürkle, F. Pauly, J. C. Cuevas, M. Mayor, T. Wandlowski, *J. Am. Chem. Soc.* **2011**, *133*, 184-187.

[12] C. J. Lambert, *Chem. Soc. Rev.* **2015**, *44*, 875-888.

[13] A. Al-Backri, V. Zólyomi, C. J. Lambert, *J. Chem. Phys.* **2014**, *140*, 104306.

[14] E. Mostaani, B. Monserrat, N. D. Drummond, C. J. Lambert, *Phys. Chem. Chem. Phys.* **2016**, *18*, 14810-14821.

[15] G. Kastlunger, R. Stadler, *Phys. Rev. B* **2013**, *88*, 035418.

[16] M. Kamenetska, S. Y. Quek, A. C. Whalley, M. L. Steigerwald, H. J. Choi, S. G. Louie, C. Nuckolls, M. S. Hybertsen, J. B. Neaton, L. Venkataraman, *J. Am. Chem. Soc.* **2010**, *132*, 6817-6821.